Journal of Applied Polymer Science

Crystallization Kinetics and Phase Transformation of Poly(vinylidene fluoride) Films Incorporated with Functionalized $BaTiO_3$ Nanoparticles

Hui-Jian Ye,[1] Wen-Zhu Shao,[1] Liang Zhen[1,2]

[1]School of Materials Science and Engineering, Harbin Institute of Technology, Harbin 150001, People's Republic of China
[2]MOE Key Laboratory of Micro-system and Micro-structures Manufacturing, Harbin Institute of Technology, Harbin 150080, People's Republic of China
Correspondence to: L. Zhen (E-mail: lzhen@hit.edu.cn)

ABSTRACT: The transformation of α to β-phase in poly(vinylidene fluoride) (PVDF) induced by the addition of tetradecylphosphonic acid (TDPA)-$BaTiO_3$ nanoparticles and subsequently the isothermal crystallization kinetics of pristine PVDF and its nanocomposites have been investigated. The result of infrared spectra showed that the relative crystalline fraction of β-phase was enhanced greatly after the introduction of TDPA–$BaTiO_3$ nanoparticles, and reached the peak of 93% when the concentration of nanofillers was 20%. The interaction between TDPA–$BaTiO_3$ nanoparticles and PVDF macromolecular chains induced the change of conformation from *trans-gauche* to all-*trans* crystal structure in PVDF segment. The isothermal crystallization of TDPA–$BaTiO_3$/PVDF nanocomposites was carried out by the differential scanning calorimetry (DSC). The influence of TDPA–$BaTiO_3$ nanoparticles concentration on crystallization rate, activate energy, melting enthalpy, and peak temperature were studied. The nanocomposite film loaded 20% TDPA–$BaTiO_3$ nanoparticles exhibited the highest crystallization rate and activate energy, which decreased after loading more nanofillers in the host because of high volume fraction of nanoparticles leading to steric hindrance and further weakening the mobility of PVDF chains during the crystallization. © 2013 Wiley Periodicals, Inc. J. Appl. Polym. Sci. 129: 2940–2949, 2013

KEYWORDS: crystallization; phase behavior; kinetics; PVDF

Received 27 August 2012; accepted 13 December 2012; published online 15 February 2013
DOI: 10.1002/app.38949

INTRODUCTION

Dielectric materials play a key role in modern energy storage system and have expansive applications from electric storage to energy transformation energy.[1–3] Due to increasing demands for compact electronics and electric storage devices with high energy density, the development of dielectric materials with high permittivity becomes the hot issue of present research. Such as, dielectric capacitors with high energy density can significantly reduce the weight, the volume and the cost of entire energy storage system. Dielectric polymers are the primary choice for energy storage capacitors owing to wonderful mechanical flexibility, high dielectric strength, low cost, and also processing advantages.[4–8]

Discovery of poly(vinylidene fluoride) (PVDF) with greatly enhanced ferroelectric property opened a new world of ferroelectric polymer science, and since then PVDF has established itself as a vital ferroelectric polymer.[1,9] PVDF exhibits a very simple chemical formula, and its constitutional repeating unit is —CH_2—CF_2—, intermediate between polyethylene (PE) —CH_2—CH_2— and polytetrafluoroethylene (PTFE) —CF_2—CF_2—. This similarity of chemical structure guarantees both great mechanical flexibility (as much as PE) and steric constraint (as seen in PTFE) of PVDF chains. Because of these structure characteristics, there are many types of geometric configuration and crystal structure in PVDF, depending on processing conditions during fabrication of PVDF. Given the packing modes of these molecular chains into the unit cell, macromolecular conformations of PVDF appear in four kinds of crystalline phases known as α, β, γ, and δ. In view of practical applications the α- and β-phases are the most important crystalline structures. The α-phase belongs to *trans-gauche* (TGTG') conformation and is nonpolar. Therefore the α-phase crystalline form of PVDF exhibits low permittivity. It can be commonly obtained from molten sample cooled to room temperature at a normal cooling rate or solvent cast at solvent evaporation temperature above 120°C. The β-phase with all-*trans* bond (TTTT) conformation is comprised of fluoride and hydrogen atoms on the opposite sides of the polymer chains, which leads to net dipole moment.[9] The unit cell of β-phase contains two identical all-*trans* chains packed with their dipoles having same direction and being perpendicular to the polymer main chain. This provides great piezoelectricity and ferroelectric, which are important to the applications of energy conversion and

storage involving the electroactive properties of dielectric materials.

Generally, the β-phase PVDF is transformed by stretching the α-phase at the temperature below 100°C with a stretch factor between 3 and 5.[10–12] The solvent evaporation temperature of unoriented β-phase PVDF obtained by solution cast usually below 70°C. If the preparation temperature is higher than 70°C, the sample will be mixtures containing both α- and β-phases, and the fraction of α-phase increases with increasing solvent evaporation temperature. The crystal form of PVDF membrane was β-phase and displayed high permittivity in some specific solvents. Also the PVDF films in different types of diluents, such as 1,2-propylene glycol carbonate, dimethyl phthalate, diphenyl ketone, and dibutyl phthalate by the thermally induced phase separation method exhibited three kinds of morphologies.[13]

The crystal structure and physical properties of PVDF not only depend on the prepared conditions but also can be strongly affected by the presence of nanoparticles, which effects on the crystallization behavior and polymer morphology.[14–16] Influence of nanofillers, such as carbon nanofibers and magnetic nanoparticles on the transformation of α to β-phase has been studied. Lanceros-Mendez et al.[17] investigated the effect of carbon nanofiber concentration on the transformation of α to β-phase of PVDF matrix. The stretching of as-prepared composite films by solution casting induced the transformation of α to β-phase within the polymer matrix. In this phase transformation, the polymer chains were prompted to all-*trans* zigzag conformation and oriented in the crystals. This phase transformation occurred as in the plain PVDF with the destruction of the spherulitic microstructural morphology and then produced a microfibrillar one. Moreover, the addition of the carbon nanofibers in the PVDF matrix increased the degree of crystallinity of the polymer composites. The influence of the existence of multiwalled carbon nanotubes on the formation of β-crystalline phase in the PVDF host was studied by Song et al.[18] The fraction of β-phase can be greatly enhanced with wrapped carbon nanotubes. Piezoelectric property of PVDF and carbon nanotubes blends was investigated by Hong et al.[19] The enhancement of the elastic modulus property can be explained by the transformation of α to β-phase in the polymer microstructure due to the presence of carbon nanotubes. Furthermore, the existence of nanoparticles also influence on crystallization kinetics. Despite the crystallization behavior of α-phase PVDF have been studied,[20] the effect of nanoparticles on the crystallization of polymer-based dielectric nanocomposite has not investigated in-depth.

Recent researches show that the addition of nanoparticles into the PVDF matrix shifts the crystallization peak to higher temperature, and also smaller spherulites of PVDF were produced. This indicates that the crystallization rate of PVDF accelerates in the blends because of the nucleating function of nanoparticles.[21] Ferrite nanoparticles, such as magnetic carbon nanotubes, $CoFe_2O_4$ and $NiFe_2O_4$ were added into polymer matrix via solution blending with different concentrations to obtain ferrite nanoparticles/polymer nanocomposite.[22–24] The used ferrite nanoparticles played a key role in nucleating the ferroelectric phase of PVDF. The nucleation kinetics of nanocomposites was enhanced by the existence of $CoFe_2O_4$ and $NiFe_2O_4$ nanoparticles. There was a key change in Avrami's exponent with increasing nanoparticles concentration. Nandi et al.[25] made use of nano-sized Ag to act as nuclei in the crystallization of β-crystalline phase PVDF. The melting point and enthalpy of fusion of PVDF in the nanocomposite enhanced with increasing in Ag nanoparticles concentration. The crystallization indicates nucleating effect of Ag nanoparticles in the composite.

Regarding isothermal crystallization kinetics of polymer nanocomposites, Papageorgiou coworkers[26] took advantage of Avrami equation, demonstrated that crystallization rates of silica/poly(propylene terephthalate) nanocomposites were enhanced with low silica content. The reduced recrystallization on heating was observed due to bonding between the cross-linking of the polymer macromolecules and silica nanoparticles. More recently, ferroelectric ceramic nanoparticles were added into PVDF matrix to improve the dielectric property and meet the increasing demand of advanced applications in up-to-date electronics and energy storage.[27–32] The addition of ferroelectric nanoparticles enhanced the permittivity of polymer nanocomposites. Nevertheless, the transformation of different crystal types in the PVDF matrix induced by ferroelectric nanoparticles has not been studied extensively. The crystallization behavior of this nanocomposite film needs to be investigated further.

In this work, we report a simple and convenient method to fabricate tetradecylphosphonic acid (TDPA)-$BaTiO_3$/PVDF nanocomposite films with different concentrations by casting solution. The used nanoparticles induce the transformation of α to β-phase in PVDF matrix. Furthermore, the crystallization kinetics of PVDF nanocomposites has been studied to investigate the effect of nanoparticles during the crystallization in the different crystal phases.

EXPERIMENTAL

Materials

PVDF powder was purchased from Shanghai 3F Company (China). Barium titanate (99+%, 60–80 nm) nanoparticles was bought from Aldrich and functionalized with TDPA which was synthesized according to Arbuzov reaction. TDPA–$BaTiO_3$ nanoparticles were used as active nanofillers in PVDF nanocomposite films. *N*, *N*-dimethylacetamide (DMAc) was purchased from Sinopharm Chemical Reagent Company (China), and used without further purification.

Preparation of PVDF Nanocomposite Films

The film in a thickness of 55–60 μm was prepared via casting the PVDF solution in DMAc on glass plate followed by drying at 60°C for 120 min. The PVDF powder (0.5 g) was initially dissolved in 10 mL DMAc. After stirring the mixture for 30 min, the TDPA–$BaTiO_3$ nanoparticles were added in. The mixed solution was stirred for 25 min at room temperature and ultrasonicated for 10 min to make sure TDPA–$BaTiO_3$ nanoparticles dispersing homogenously in solution. To remove extra gas in

Applied Polymer SCIENCE

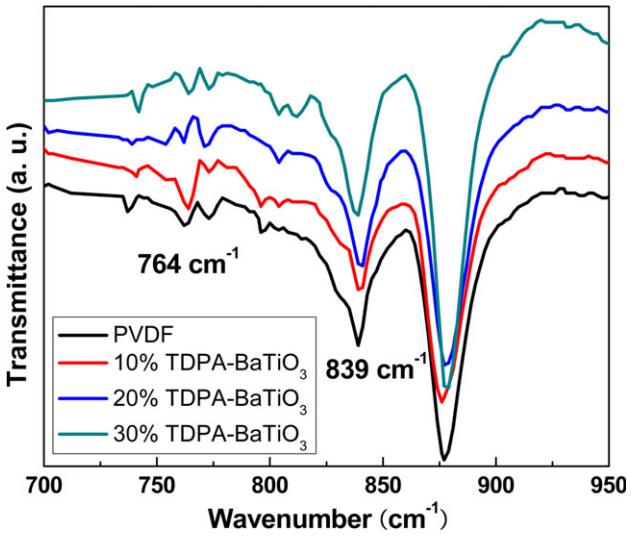

Figure 1. FT-IR spectra of PVDF and its nanocomposites with different concentrations of TDPA–$BaTiO_3$ nanoparticles. [Color figure can be viewed in the online issue, which is available at wileyonlinelibrary.com.]

the solution, the mixture was stewed for 20 min before pouring on glass substrate, which was dried at 60°C for 120 min and cooled slowly to room temperature.

FT-IR Analysis

Infrared measurements were performed to determine and characterize the presence of the different PVDF crystalline phase. A Nicolet Avartar 360 apparatus was used in transmittance mode and Fourier transform infrared spectra (FT-IR) were collected with a resolution of 2 cm^{-1} from 4000 to 600 cm^{-1}.

Isothermal Crystallization Kinetics

Crystallization kinetics of PVDF and its nanocomposite films was measured by isothermal experiments using differential scanning calorimetry (DSC, TA Q2000). Dry high-purity nitrogen gas was sent into DSC cell through the whole experiment with a flow rate of 50 mL per minute. The sample of each nanocomposite, cut from the film, around 5 mg, was sealed in aluminum pans and used for the entire isothermal experiments. Nearly, all the samples had the equally weight (about 5 mg) and the identical thickness, around 60 μm. The thermal history of PVDF nanocomposite films were erased by heating at 180°C for 3 min. The samples then were quenched at the fastest rate (around 45°C/min) to the chosen isothermal crystallization temperature T_c (from 144 to 148°C) and held at it for 15 min. The samples were then cooled to ambient temperature and heated to 180°C at 10°C/min. The calibration of the DSC was made with the standard calibration of TA Q series.

RESULTS AND DISCUSSION

Content of β-Phase in the PVDF and Nanocomposite Films

As already reported in previous works, the addition of nanofillers, such as carbon nanotubers or magnetic nanoparticles, changes the crystallization behavior of the host polymers.[33,34] In this work, PVDF nanocomposites were prepared via simple solution casting with different contents of TDPA–$BaTiO_3$ nanoparticles in the polymer matrix to explore the effect of nanofillers during the crystallization and the phenomenon of TDPA–$BaTiO_3$ nanoparticles inducing crystallization of the β-phase PVDF directly.

The FT-IR spectra for PVDF with different contents of TDPA–$BaTiO_3$ nanoparticles were shown in Figure 1. The infrared transmittance bands at 764 and 839 cm^{-1} represent α and β-phase of PVDF, respectively. It is observed that both α and β-phase exist in the neat PVDF and its nanocomposite films. The higher content of nanofillers in the nanocomposite comprised, the higher crystallinity of β type structure was formed.

The relative content of β-phase in each sample was examined from the infrared transmittance bands at 764 and 839 cm^{-1}. It is estimated that the relative fraction of β-phase can be calculated by eq. (1), assuming that the infrared transmittance obeys the Lambert-Beer law.[35]

$$F(\beta) = \frac{X_\beta}{X_\alpha + X_\beta} = \frac{A_\beta}{(K_\beta/K_\alpha)A_\alpha + A_\beta} \quad (1)$$

where A_α and A_β are the absorbance at 764 and 839 cm^{-1}, respectively, and K_α and K_β represent the absorption coefficients at the corresponding wavenumber, which are 6.1×10^4 and 7.7×10^4 cm^2 mol^{-1}. For the nanocomposite films, the variation of relative fraction of β-phase with increasing concentration of TDPA–$BaTiO_3$ nanoparticles was depicted in Figure 2. In the pristine PVDF film, the relative crystalline fraction of β-phase was 66%. According to previous researches, the evaporation temperature during the fabrication of nanocomposite film affected the form of different crystal structures.[34] In this study, the temperature of film fabrication was 60°C and under such evaporation temperature PVDF macromolecular segments are likely to produce all-*trans* zigzag conformation. After adding the nanofillers into PVDF host, the relative crystalline fraction of β-phase increased, which arrived at the peak of 93% while the concentration of TDPA–$BaTiO_3$ nanoparticles was 20%. Obviously, the used

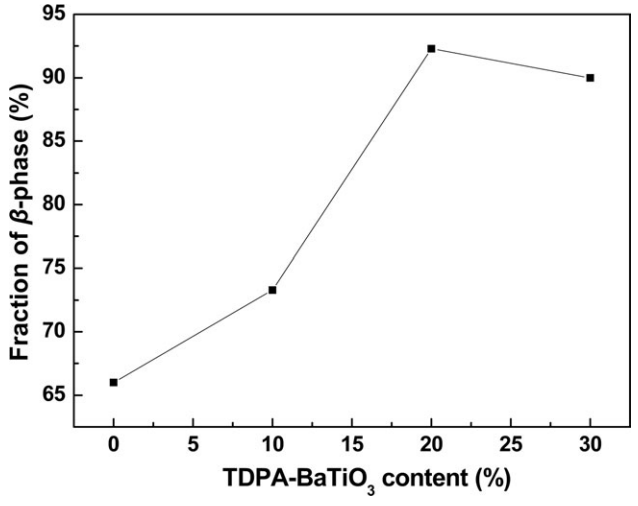

Figure 2. Evolution of the β-phase content with increasing TDPA–$BaTiO_3$ nanoparticles content.

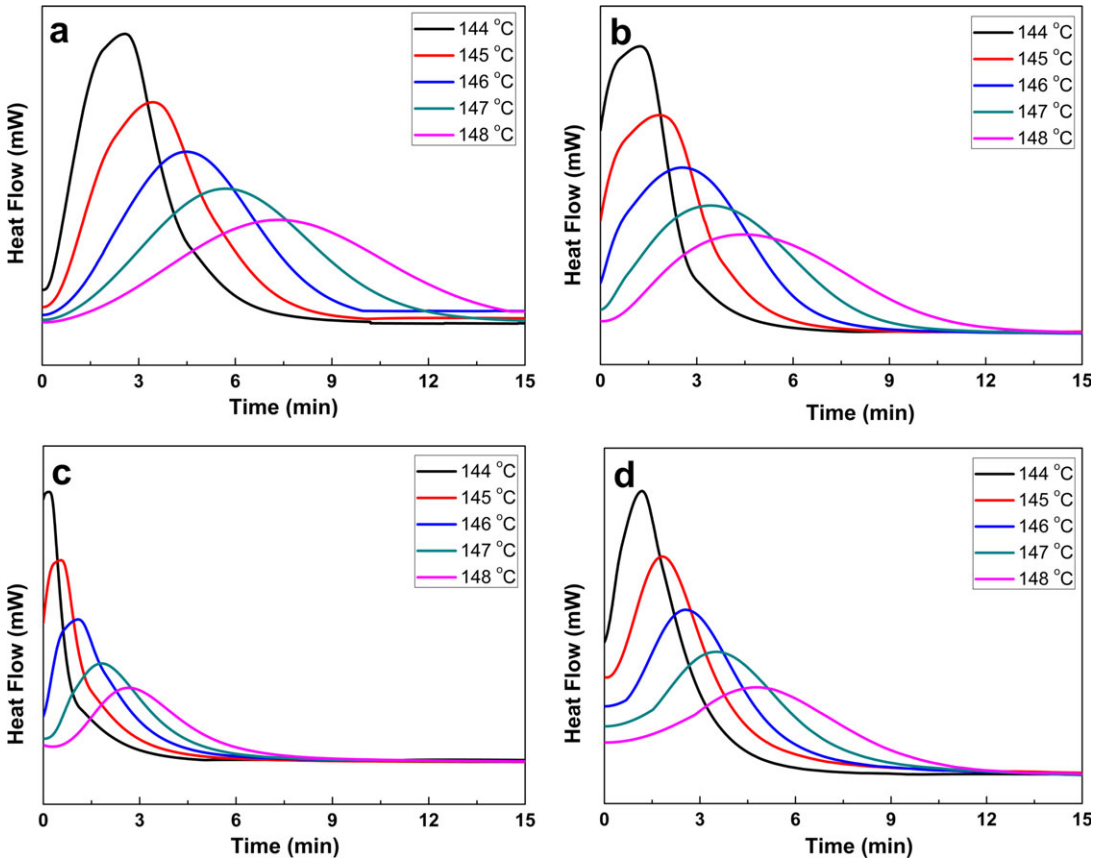

Figure 3. Crystallization thermograms at 144–148°C for different concentrations of PVDF nanocomposite films: (a) pristine PVDF film; (b) 10% TDPA–$BaTiO_3$; (c) 20% TDPA–$BaTiO_3$; (d) 30% TDPA–$BaTiO_3$. The exothermal peak is up. [Color figure can be viewed in the online issue, which is available at wileyonlinelibrary.com.]

nanoparticles enhanced the content of β-phase in the nanocomposites. The interaction between nanoparticles and PVDF chains induced the change of the all-*trans* conformation in PVDF segment. The existence of TDPA–$BaTiO_3$ nanoparticles promoted the all-*trans* nucleation of PVDF segment, and then this structure propagated in the crystal growth of PVDF chains. In this work, the demonstrating by FT-IR spectra indicated the greatly enhancement of β-phase crystallinity with the presence of TDPA–$BaTiO_3$ nanoparticles.

Crystallization Behavior of PVDF and Its Nanocomposite Films

All isothermal crystallization experiments were conducted on each sample in the aluminum pan of the DSC cell during the entire experiment. After the first melting, the repeatability is excellent. For instance, melting and cool cycles of 10% nanofillers nanocomposite film go for five times and the difference in the endothermal peak position is smaller than 0.2% while the difference in the crystalline fraction which was determined by the integration of the peak was smaller than 1.3%. Repeatability of a series of different samples was examined with two sealed samples of the same volume fraction nanocomposite film for melting and crystallization cycles. Uncertainty of endothermic peak temperature is still less than 0.3% and difference of crystallization fraction is less than 2.5%. This also indicates that the nanoparticles dispersed well in the nanocomposite films.

Typical DSC isothermal crystallization of pristine PVDF and its nanocomposites were exhibited in Figure 3. The maximum exothermal peak shifts toward longer time as the isothermal

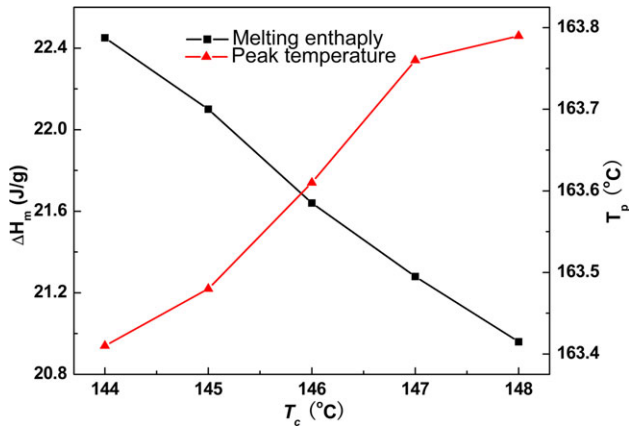

Figure 4. Dependence of melting enthalpy (■) and peak temperature (▲) of pristine PVDF on crystallization temperature. [Color figure can be viewed in the online issue, which is available at wileyonlinelibrary.com.]

Table I. Evolution of Melting Enthalpy and Peak Temperature of PVDF and Its Nanocomposite Films

T_c(°C)		144	145	146	147	148
PVDF	ΔH_m (J/g)	22.45	22.10	21.64	21.28	20.96
	T_p (°C)	163.41	163.48	163.61	163.76	163.79
10% TDPA-$BaTiO_3$	ΔH_m (J/g)	20.27	19.93	19.76	19.63	19.41
	T_p (°C)	163.64	163.81	163.97	164.04	164.15
20% TDPA-$BaTiO_3$	ΔH_m (J/g)	9.73	9.54	9.38	9.20	9.06
	T_p (°C)	163.00	163.22	163.36	163.39	163.48
30% TDPA-$BaTiO_3$	ΔH_m (J/g)	5.76	5.71	5.65	5.46	5.34
	T_p (°C)	162.74	162.91	162.98	163.03	163.20

crystallization temperature increases. The same trend was observed in the isothermal crystallization of PVDF nanocomposite films [Figure 3(b–d)]. At higher temperature, polymer chain exhibits high mobility and needs more time to propagate regular crystal structure. At certain isothermal temperature the peak moves to shorter time as content of nanoparticles increases, and then moves to longer time when the nanocomposite film containing 30% TDPA–$BaTiO_3$ nanoparticles. Nucleation of TDPA–$BaTiO_3$ nanoparticles reduces the time of crystallization at low concentration. At higher content in the nanocomposite film, besides of nucleation, the existence of nanoparticles result in steric hindrance. Polymer chains have to overcome the hindrance in the initial stage of crystallization, so it takes longer time to pack into the regular crystal structure.

The crystallization fraction was calculated from the integration of the endothermic peaks, assuming that the melting enthalpy of the 100% crystalline α-PVDF is 93.07 J/g.[36] The Melting enthalpy and peak temperature for pristine PVDF was represented in Figure 4 and for PVDF nanocomposite films were listed in Table I. The peak temperature of PVDF nanocomposites increased with the rising crystallization temperature. The

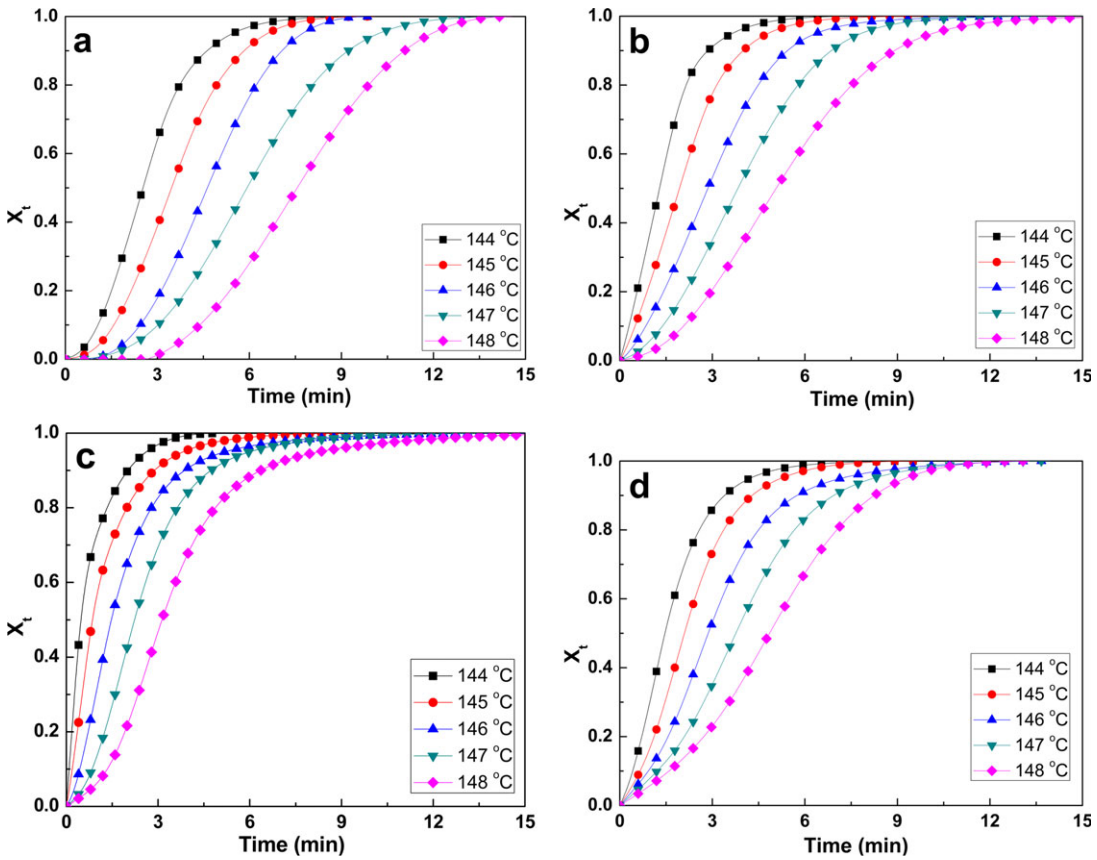

Figure 5. Evolution of relative degree of crystallinity as a function of crystallization time at various isothermal temperatures for different contents of nanoparticles: (a) pristine PVDF film; (b) 10% TDPA–$BaTiO_3$; (c) 20% TDPA–$BaTiO_3$; (d) 30% TDPA–$BaTiO_3$. [Color figure can be viewed in the online issue, which is available at wileyonlinelibrary.com.]

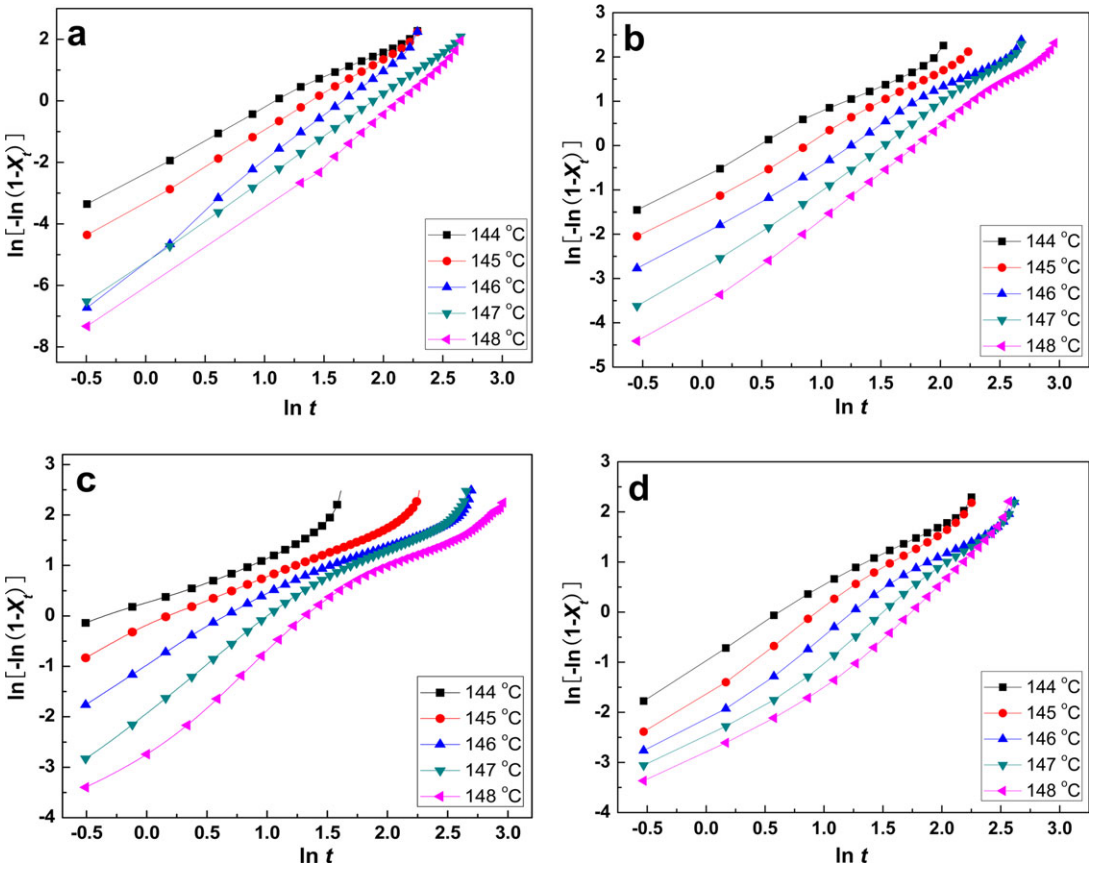

Figure 6. Avrami plots $[\ln(1 - X_t)]$ against ln t at various temperatures for different contents of nanoparticles: (a) pristine PVDF film; (b) 10% TDPA–$BaTiO_3$; (c) 20% TDPA–$BaTiO_3$; (d) 30% TDPA–$BaTiO_3$. [Color figure can be viewed in the online issue, which is available at wileyonlinelibrary.com.]

crystallization fraction of PVDF reduced slightly with the increasing isothermal temperature. While the following melting peak temperature increased a little with increasing crystallization temperature. In the whole crystallization of polymers usually there are two stages, nucleation and crystal growth, respectively. The crystalline rate was controlled by those two stages. At high crystalline temperature, the size of polymer crystal is larger because of low super cooling. In the opposite, the crystalline size will be smaller at low crystalline temperature under high super cooling. Thus the melting enthalpy decreased with increasing temperature. The crystalline fraction of PVDF in the sample decreased obviously as the content of TDPA–$BaTiO_3$ nanoparticles increased. This phenomenon can be explained that the heterogeneous nucleation of TDPA–$BaTiO_3$ nanoparticles effect on the movement of PVDF macromolecular chain segments, and PVDF host and the nanofillers can be likely to be uniform system, which leads to the crystallinity of PVDF decreases at a high nanoparticles volume fraction. This was also evidenced by the isothermal crystallization of poly(vinyl methyl ether) aqueous solution and ferrite nanoparticles/PVDF.[24,37] This fact is contrast to some fillers such as carbon black,[38] silica nanoparticles,[39] and vapor grown carbon nanofibers[17] that are reported to increase the crystalline fraction of polymer. In this study, the used nanoparticles with a constrained polymer layer act as nucleating agents and affect the crystallization kinetics instead of acting as heterogeneous nucleating agents.[40] This shows that the presence of nanoparticles has a complex effect on the crystallization of PVDF.

Crystallization Kinetics of the Nanocomposite Films

Crystallization kinetics of polymer nanocomposites depends on various influencing factors. For example, the nucleation of polymer chains, interaction between macromolecular chain and nanoparticles surfaces, and the coexistence of different crystalline phases caused by varied nucleation and crystal growth rates have important effects on the crystallization kinetics of polymer nanocomposite. To further analyze the isothermal crystallization experiments, the crystallization of PVDF and its nanocomposites was compared. Analysis of the overall crystallization rate under isothermal experiment is generally accomplished with the use of Avrami equation that was used in the crystallization of metals at first, now applied in the crystallization kinetics of polymers widely.

A general form of Avrami equation is described as:[41–43]

$$1 - X_t = \exp(-Kt^n) \quad (2)$$

where X_t is relative degree of crystallinity, while K and n are constants of a given morphology and type of nucleation. K is

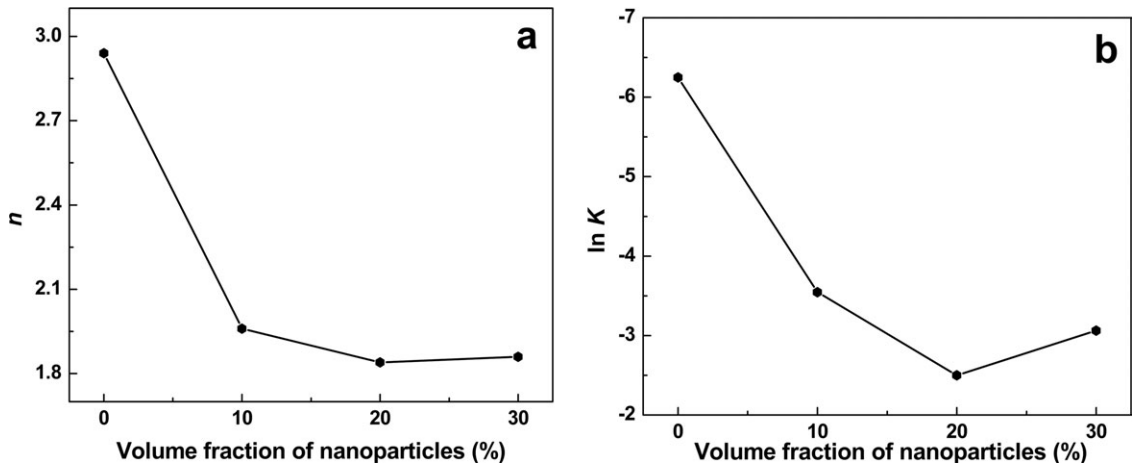

Figure 7. Evolution of the Avrami parameters: (a) n and (b) ln K with different volume fraction of TDPA–$BaTiO_3$ nanoparticles. The isothermal crystallization temperature is 148°C.

crystallization rate constant, while n is Avrami index and includes information of nucleation and growth geometry. The exponent, n, is correlated to space dimensionality of growth and time dimensionality of nucleation. The determination of n values is complicated by factors such as more than single mode of nucleation, various morphologies in growth of crystal, incomplete crystallization, or phase transformation involved during the process. Thus values of n are always fractions instead of integers.

As discussed before, the addition of nanoparticles has a complex effect on the crystallization of PVDF. Now the influence of nanoparticles on the kinetics of PVDF crystalline with the Avrami equation is examined. X_t is relative degree of crystallinity, as a function of crystallization time t, and can be defined as:

$$X_t = \frac{\int_0^t \left(\frac{\partial H}{\partial t}\right)\partial t}{\int_0^\infty \left(\frac{\partial H}{\partial t}\right)\partial t} \tag{3}$$

where $\partial H/\partial t$ is the DSC heat flow. The numerator means the enthalpy at a given time t, and the denominator is the total exothermal enthalpy when the crystallization is completed. The development of crystallinity X_t as a function of time, t, for PVDF and its nanocomposites at various crystallization temperatures were shown in Figure 5, which were represented by different geometrical symbols. S-shaped curves were obtained, which are consistent with nucleation and growth process of polymer crystallization. At the lower crystallization temperature, less time needed to achieve the end of crystallization. For example, the crystallization of neat PVDF almost completed after 6 min at 144°C, however, under the same time at the crystallization temperature of 148°C the relative degree of crystallinity reached 28%. In addition, we found that no matter which temperature chosen for 20% TDPA–$BaTiO_3$ nanoparticles nanocomposite film, it needs the least time to complete the crystallization. Even at 148°C when the crystallization time reached 6 min, >90% crystallinity was finished.

Under the crystallization temperature of 148°C, at the initial stage of isothermal crystallization, the nuclei of pristine PVDF needs more time, and the X_t is very small. After adding the nanoparticles into PVDF matrix, at certain time the relative degree of crystallinity is raised. During the whole crystallization time, the X_t of nanocomposites are higher than it of pristine PVDF. The presence of TDPA–$BaTiO_3$ nanoparticles turned the crystallization of PVDF from homogeneous to heterogeneous nucleation. Also the addition of nanoparticles promotes the nuclei of PVDF chain segments and reduces the time of pregnant period, thus the X_t of PVDF nanocomposite films are higher than that of pristine PVDF at given time. Meanwhile the existence of nanoparticles is too much in the host, like volume fraction of 30%, the crystallization of PVDF will be hindered.

Applying logarithmic properties to both sides of eq. (2), the linearized equation can be obtained:

$$\ln[-\ln(1 - X_t)] = \ln K + n\ln t \tag{4}$$

The above mentioned equation represents that n is the slop of the plot of $[\ln(1 - X_t)]$ against ln t. Figure 6 shows this representation for PVDF and its composites with different volume fractions of TDPA–$BaTiO_3$ nanoparticles under various crystallization temperatures. Applying the eq. (4), the influence of nanoparticles on the Avrami parameters of crystallization of PVDF is shown in Figure 7. There is an important change in Avrami exponent which reduces from 2.9 to around 2.0 with the increasing TDPA–$BaTiO_3$ nanoparticles at 148°C, and the similar trend happens to the crystallization rate constant K. The connection of macroscopic Avrami parameters and microscopic polymer chain crystal interaction is that both nucleation kinetics and the interaction of growing polymer crystal leads to changes in kinetics parameters. This shows the existence of nanoparticles has a vital effect on the crystallization of PVDF.[17,24]

The half crystallization time, $t_{1/2}$, is defined as the time when the extent of crystallization reached 50% of overall. It can be obtained from eq. (2):

$$1/2 = 1 - X_t = \exp(-Kt^n) \tag{5}$$

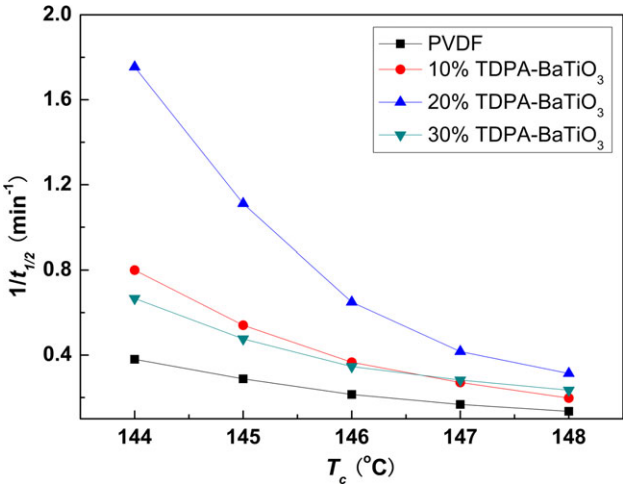

Figure 8. Plots of the reciprocal half crystallization time versus temperature during isothermal crystallization of pristine PVDF and TDPA–$BaTiO_3$/PVDF nanocomposites. [Color figure can be viewed in the online issue, which is available at wileyonlinelibrary.com.]

that can be further rewritten as:

$$t_{1/2} = \left(\frac{\ln 2}{K}\right)^{1/n} \tag{6}$$

where $t_{1/2}$ is the time at which the extent of relative crystallization is 50%. It can be considered approximately as the growth rate of crystallization (Figure 8). The isothermal crystallization parameters of PVDF and its nanocomposite films at various crystallization temperatures were shown in Table II.

Nucleation plays a key part in the kinetics of mass crystal growth that was observed by DSC thermograms. Generally, the mass crystal growth increases with increasing nucleation under the same crystal growth rate at the first period of crystallization when the spherulites collide with each other. The growth rate of crystallization for plain PVDF was below 0.4 min^{-1} at the crystallization temperature of 144°C. After adding TDPA–$BaTiO_3$ nanoparticles into PVDF matrix, it increased greatly and reached the peak of 1.8 min^{-1} for 20% TDPA–$BaTiO_3$ nanoparticles nanocomposite film. Loading more nanoparticles into films, the crystal growth rate decreased deeply. Because too much nanoparticles loaded in the nanocomposite hinders the reorganization of PVDF macromolecule chain. At high crystallization temperature, such as 148°C, the growth rate of crystallization for various concentrations had little difference. It indicates that the growth of crystal is a key step for the overall crystallization at high temperature.[44,45]

Activate Energy of the Nanocomposite Films in Crystallization

Assuming that the isothermal crystallization is activated by thermal, crystallization rate constant, K, can be applied by Arrhenius equation:[46]

$$K^{\frac{1}{n}} = k_0 \exp\left(-\frac{\Delta E}{RT_c}\right) \tag{7}$$

that can be further expressed as:

$$\frac{1}{n}\ln K = \ln k_0 = \frac{\Delta E}{RT_c} \tag{8}$$

where k_0 is a temperature-independent pre-exponential factor, R the gas constant, T_c isothermal temperature, and ΔE is the crystallization activate energy. ΔE can be determined by the slope coefficients of plots of $(1/n)\ln K$ as a function of $1/T_c$ (Figure 9). The effect of the TDPA–$BaTiO_3$ nanoparticles contents on the activate energy of isothermal crystallization of PVDF was exhibited in Figure 10. It can be observed that the crystallization

Table II. Isothermal Crystallization Parameters for PVDF and Its Nanocomposite Films at Various Crystallization Temperatures

T_c (C)		144	145	146	147	148
PVDF	n	1.96	2.34	3.11	2.73	2.94
	ln K	−2.2648	−3.2759	−5.1503	−5.2439	−6.2480
	$t_{1/2}$	2.63	3.47	4.66	5.97	7.39
	R^2	0.9963	0.9990	0.9979	0.9998	0.9920
10% TDPA-$BaTiO_3$	n	1.37	1.50	1.58	1.86	1.96
	ln K	−0.6754	−1.2879	−1.9533	−2.7937	−3.5445
	$t_{1/2}$	1.25	1.85	2.73	3.69	5.06
	R^2	0.9947	0.9985	0.9956	0.9981	0.9978
20% TDPA-$BaTiO_3$	n	1.03	1.02	1.19	1.55	1.84
	ln K	0.2211	−0.2615	−0.8777	−1.7207	−2.4998
	$t_{1/2}$	0.57	0.90	1.54	2.40	3.19
	R^2	0.9634	0.9946	0.9871	0.9871	0.9925
30% TDPA-$BaTiO_3$	n	1.37	1.61	1.54	1.72	1.86
	ln K	−0.9206	−1.5595	−2.0032	−2.5418	−3.0632
	$t_{1/2}$	1.50	2.10	2.89	3.54	4.26
	R^2	0.9943	0.9971	0.9924	0.9916	0.9727

activate energy of TDPA–$BaTiO_3$/PVDF nanocomposites is higher than plain PVDF. It exhibits an increasing trend with loading up to 20% and decreases at 30% TDPA–$BaTiO_3$ nanoparticles nanocomposite. This is probably because the crystallization of PVDF concludes both nucleation and crystal growth. For the neat PVDF, the nucleation of PVDF is the key stage in the crystallization. When the content of nanofillers reaches 20%, the strong nucleation effect of nanoparticles plays an important role in the crystallization of PVDF nanocomposite. At higher concentration, the presence of nanoparticles leads to more steric hindrance than nucleation effects, thus reducing the mobility of PVDF polymer chains during the crystallization. This also explains that the fraction of β-phase with the 20% TDPA–$BaTiO_3$ nanoparticles nanocomposite film is the highest. The surface functionalization of $BaTiO_3$ nanoparticles may have huge influence on the crystallization of polymer host. Because of interaction between the polymer and functional groups, the thermal property of PVDF host was affected by the functional groups on the surface of $BaTiO_3$ nanoparticles.[47] Therefore, the activate energy of crystallization increases after adding the nanoparticles into PVDF matrix, which was also proved in other polymer-based composites.[48]

CONCLUSIONS

In conclusion, the evolution of different crystal structures prompted by TDPA–$BaTiO_3$ nanoparticles and the isothermal crystallization of PVDF and its nanocomposite films have been studied. It has been proved that the addition of TDPA–$BaTiO_3$ nanoparticles induces the transformation of α-phase to β-phase. The fraction of β-phase was 66% in the pristine PVDF film while it increased to the peak of 93% at 20% TDPA–$BaTiO_3$ nanocomposite film. In the blends the existence of TDPA–$BaTiO_3$ nanoparticles promoted the all-*trans* nucleation of PVDF segment, and then this structure grew in the crystal growth of PVDF chains to form β-phase in nanocomposite film. According to the isothermal crystallization examination of TDPA–$BaTiO_3$/PVDF nanocomposite films, the maximum exothermal peak shifts toward longer time with increasing isothermal crystallization temperatures. The reduce of degree of crystallinity for PVDF with increasing concentration of nanoparticle is observed, implying that a portion of macromolecular chains are confined in interphases with the nanofillers and are unlikely to diffuse and grow into regular crystals. The nucleation kinetics is enhanced by the existence of nanoparticles and there is a significant change in Avrami exponent occurs with increasing concentration of nanoparticle. The nanocomposite film loaded 20% TDPA–$BaTiO_3$ nanoparticles exhibited the highest crystallization rate and activate energy as a consequence of nucleation effect of TDPA–$BaTiO_3$ nanoparticles, which may lead to the highest content of β-phase. At higher concentration, like 30% TDPA–$BaTiO_3$ nanoparticles, the presence of nanoparticles caused steric hindrance instead of nucleation effects and weak mobility of PVDF polymer chains during the crystallization, thus the crystallization rate and activate energy decreased.

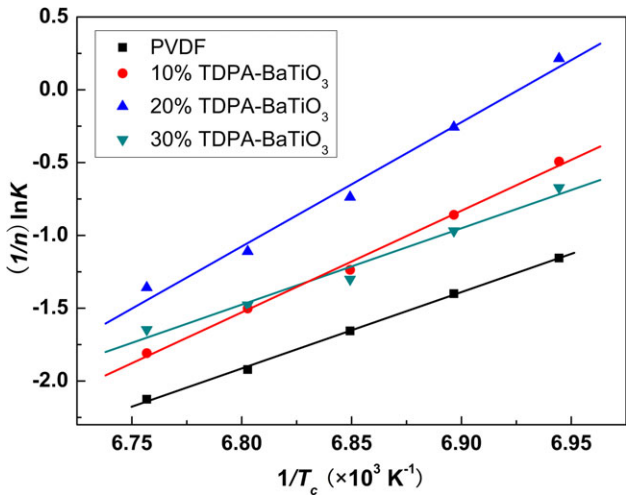

Figure 9. Plots of $(1/n)\ln K$ as a function of $1/T_c$ for PVDF and its nanocomposites. [Color figure can be viewed in the online issue, which is available at wileyonlinelibrary.com.]

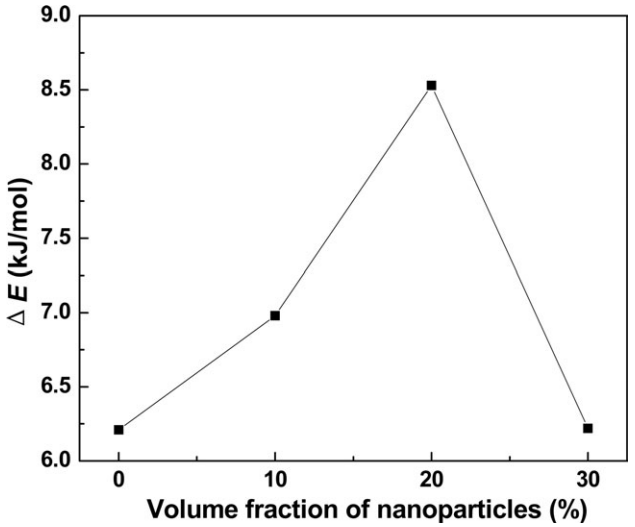

Figure 10. Effect of the TDPA–$BaTiO_3$ nanoparticles contents on isothermal crystallization activate energy of pristine PVDF.

ACKNOWLEDGMENTS

This work was financially supported Program of Excellent Team at Harbin Institute of Technology. Hui-Jian Ye acknowledges Dr. Cheng-Yan Xu for his comments and English correction and proofreading.

REFERENCES

1. Wang, Y.; Zhou, X.; Chen, Q.; Chu, B. J.; Zhang, Q. M. *IEEE Trans. Dielectr. Electri. Insul.* **2010**, *17*, 1036.
2. Li, Y. J.; Zhang, L.; Ducharme, S. *Appl. Phys. Lett.* **2007**, *90*, 132901.
3. Li, W. J.; Meng, Q. J.; Zheng, Y. S.; Zhang, Z. C.; Xia, W. M.; Xu, Z. *Appl. Phys. Lett.* **2010**, *96*, 192905.
4. Chu, B. J.; Zhou, X.; Ren, K. L.; Neese, B.; Lin, M. R.; Wang, Q.; Bauer, F.; Zhang, Q. M. *Science* **2006**, *313*, 334.
5. Ducharme, S. *ACS Nano* **2009**, *3*, 2447.

6. Chang, C.; Tran, V. H.; Wang, J.; Fuh, Y. K.; Lin, L. *Nano Lett.* **2010**, *10*, 726.
7. Zhang, Z. C; Meng, Q. J.; Chung, T.C. M. *Polymer* **2009**, *50*, 707.
8. Wang, Q.; Zhu, L. *J. Polym. Sci. Part B: Polym. Phys.* **2011**, *49*, 1421.
9. Lovinger, A. *Science* **1983**, *220*, 1115.
10. Sencadas, V.; Gregorio, R.; Lanceros-Me'ndez, S. *J. Macromol. Sci. B: Phys.* **2009**, *48*, 514.
11. Anjana, J.; Jayanth, K.; Mahapatra, D. R.; Kumar, H. H. *Proc. of SPIE* **2010**, *7647*, 76472C.
12. Vijayakumar, R. P.; Devang, V. K.; Ashok, M. *J. Appl. Polym. Sci.* **2010**, *117*, 3491.
13. Yang, J.; Wang, X. L.; Tian, Y.; Lin, Y.; Tian, F. *J. Polym. Sci. Part B: Polym. Phys.* **2010**, *48*, 2468.
14. Ma, W. Z.; Wang, X. L.; Zhang, J. *J. Polym. Sci. Part B: Polym. Phys.* **2010**, *48*, 2154.
15. Pramoda, K. P.; Mohamed, A.; Phang, I. Y.; Liu, T. *Polym. Int.* **2005**, *54*, 226.
16. Priya, L.; Jog, J. P. *J. Polym. Sci. B: Polym. Phys.* **2002**, *40*, 1682.
17. Costa, P.; Silva, J.; Sencadas, V.; Costa, C. M.; van Hattum, F. W. J.; Rocha, J. G.; Lanceros-Mendez, S. *Carbon* **2009**, *47*, 2590.
18. He, L.; Sun, J.; Wang, X.; Yao, L.; Li, J.; Song, R.; Hao, Y.; He, Y.; Huang, W. *J. Colloid Interface Sci.* **2011**, *363*, 122.
19. Kim, G. H.; Hong, S. M.; Seo, Y. *Phys. Chem. Chem. Phys.* **2009**, *11*, 10506.
20. Sencadas, V.; Costa, C. M.; Ribelles, J. L. G.; Lanceros-Mendez, S. *J. Mater. Sci.* **2010**, *45*, 1328.
21. Barrau, S.; Vanmansart, C.; Moreau, M.; Addad, A.; Stoclet, G.; Lefebvre, J. M.; Seguela, R. *Macromolecules* **2011**, *44*, 6496.
22. Kim, T. I.; Lee, J. H.; Shofner, L. M.; Jacob, K.; Tannenbaum, R. *Polymer* **2012**, *53*, 2402.
23. García-Gutiérrez, M. C.; Nogales, A.; Rueda, D. R.; Domingo, C.; García-Ramos, J. V.; Broza, G.; Roslaniec, Z.; Schulte, K.; Davies, R. J.; Ezquerra, T. A. *Polymer* **2006**, *47*, 341.
24. Sencadas, V.; Martins, P.; Pitães, A.; Benelmekki, M.; Ribelles, J. L. G.; Lanceros-Mendez, S. *Langmuir* **2011**, *27*, 7241.
25. Manna, S.; Batabyal, S. K.; Nandi, A. K. *J. Phys. Chem. B* **2006**, *110*, 12318.
26. Achilias, S. D.; Bikiaris, N. D.; Papastergiadis, E.; Giliopoulos, D.; Papageorgiou, Z. G. *Macromol. Chem. Phys.* **2010**, *211*, 66.
27. Pecharromán, C.; Esteban-Betegón, F.; Bartolomé, J. F.; López-Esteban, S.; Moya, J. S. *Adv. Mater.* **2001**, *13*, 1541.
28. Li, J. J.; Khanchaitit, P.; Han, K.; Wang, Q. *Chem. Mater.* **2010**, *22*, 5350.
29. Dang, Z. M.; Lin, Y. H.; Nan, C. W. *Adv. Mater.* **2005**, *15*, 1625.
30. Shen, Y.; Nan, C. W.; Li, M. *Chem. Phys. Lett.* **2004**, *396*, 420.
31. Bai, Y.; Cheng, Z. Y; Bharti, V.; Xu, H. S.; Zhang, Q. M. *Appl. Phys. Lett.* **2000**, *76*, 3804.
32. Kim, P; Jones, C. S.; Hotchkiss, J. P.; Haddock, N. H.; Kippelen, B.; Marder, R. S.; Perry, W. J. *Adv. Mater.* **2010**, *19*, 1001.
33. Trujillo, M.; Arnal, L. M.; Müller, J. A.; Mujica, A. M.; Navarro, U. C.; Ruelle, B.; Dubois, P. *Polymer* **2012**, *53*, 832.
34. Tan, L. C.; Chen, Y. W.; Zhou, W. H.; Ye, S. W.; Wei, J. C. *Polymer* **2011**, *52*, 3587.
35. Sencadas, V.; Gregorio, R.; Lanceros-Méndez, S. *J. Macromol. Sci. B: Phys.* **2009**, *48*, 514.
36. Nalwa, H. S. Ferroelectric Polymers: Physics, Chemistry and Applications; Marcel Dekker Inc.: London, **1995**; Vol. *1*, p 65.
37. Zhang, T. Z.; Li, T.; Nies, E.; Berghmans, H.; Ge, L. Q. *Polymer* **2009**, *50*, 1206.
38. Zhang, G. Q.; Sun, F.; Gao, L. P.; Wang, L. N.; Shao, M.; Liu, J. Q. *J. Compos. Mater.* **2007**, *41*, 1477.
39. Kim, S. H.; Ahn, S. H.; Hirai, T. *Polymer* **2003**, *44*, 5625.
40. Kaur, J.; Lee, J. H.; Shofner, L. M. *Polymer* **2011**, *52*, 4337.
41. Avrami, M. *J. Chem. Phys.* **1939**, *7*, 1103.
42. Avrami, M. *J. Chem. Phys.* **1940**, *8*, 212.
43. Avrami, M. *J. Chem. Phys.* **1941**, *9*, 177.
44. Lorenzo, A. T.; Arnal, M. L.; Albuerne, J.; Müller, A. J. *Polym. Test.* **2007**, *26*, 222.
45. Hong, S.; Zhang, X. H.; Zhang, R. Y.; Wang, L.; Zhao, J.; Han, C. C. *Macromolecules* **2008**, *41*, 2311.
46. Arrhennius S. *Philos. Mag. J. Sci.* **1896**, *41*, 237.
47. Deng, H.; Bilotti, E.; Zhang, R.; Wang, K.; Zhang, Q.; Peijs, T.; Fu, Q. *J. Appl. Polym. Sci.* **2011**, *120*, 133.
48. Liu, X.; He, A. H.; Du, K.; Han, C. C. *J. Appl. Polym. Sci.* **2010**, *119*, 162.